

The one-loop impact of a dependent mass: the role of m_3 in the C2HDM

Duarte Fontes^{*1,2} and Jorge C. Romão^{†2}

¹*Department of Physics, Brookhaven National Laboratory, Upton, NY, 11973, USA*

²*Departamento de Física and CFTP, Instituto Superior Técnico, Universidade de Lisboa, Av. Rovisco Pais 1, 1049-001 Lisboa, Portugal*

(June 23, 2022)

In the complex 2-Higgs-Doublet Model (C2HDM), the mass m_3 of the heaviest neutral scalar h_3 is usually chosen as a derived parameter. We investigate one-loop corrections to m_3 and their impact on decays of h_3 . Strikingly, very fine-tuned regions of the parameter space can be found where such corrections are large, not due to subtraction schemes, but rather due to the particular dependence of m_3 on the independent parameters. We show that even moderate corrections can have a significant impact on decays of h_3 , as they may be several times enhanced by leading-order factors.

1 Introduction

After the observation of the Higgs boson at the Large Hadron Collider (LHC) in 2012 [1, 2], it is of the utmost importance to further explore the scalar sector of particle physics. Particularly relevant is the possibility that such sector is extended when compared to that of the Standard Model (SM); examples of models with an extended scalar sector can be found e.g. in refs. [3–5]. One of the most common models—the so-called real 2-Higgs-Doublet model (2HDM), where CP is assumed to be conserved in the potential—was recently suspected of theoretical unsoundness [6]. The model that heals it in the simplest fashion—while accounting for the already observed CP violation—is the complex 2HDM (C2HDM) [7–26], where CP is explicitly violated in the scalar sector at tree-level (thus providing a new source of CP violation, as required by the three Sakharov criteria for baryogenesis [27]). Accordingly, the three neutral scalars described by the C2HDM (h_1 , h_2 , h_3) contain in general a mixture of a CP-odd component and a CP-even one. LHC searches have already excluded the possibility according to which the scalar boson discovered in 2012 is a pure CP-odd state [28–30]; yet, the scenario where it contains a CP-odd fraction is still allowed [31].

As the LHC run-3 approaches, deviations from SM predictions are anxiously expected. The absence of any undoubtable signal of new physics so far implies that such deviations shall be subtle. As a consequence, precise predictions from the theory side are necessary. These require the inclusion of one-loop electroweak corrections, which in turn require the one-loop electroweak renormalization of the model at stake. We have recently presented the one-loop renormalization of the C2HDM [24], and showed that it configures a rather unique program of renormalization. Indeed, there are more independent counterterms than independent renormalized parameters, which means that several combinations of the former can be chosen for the same set of the latter. Moreover, the parameter m_3 (corresponding to the mass of the

^{*}dfontes@bnl.gov

[†]jorge.romao@tecnico.ulisboa.pt

heaviest neutral Higgs boson, h_3) is taken as a dependent parameter, so that it cannot be fixed to be equal to the physical mass.

In this paper, we investigate the one-loop corrections to m_3 in a particular variant of the C2HDM, the Type II C2HDM. Higher order corrections to dependent masses have been discussed at length in the context of other models, such as supersymmetric extensions of the SM (cf. ref. [32] and references therein). The importance of the investigation of the higher order corrections to the mass of h_3 in the C2HDM is at least twofold: first, it allows for a refined search of h_3 , whose physical mass may contain a non-negligible one-loop contribution; secondly, it opens the possibility of calculating one-loop corrections to processes with an external h_3 . In fact, although the residue of h_3 can be set to unity (implying that the wave-function renormalization factors become trivial), there will be non-trivial contributions to the decay width of processes with an external h_3 due to the corrections to m_3 . We explicitly address the last point by considering the next-to-leading order decay width of several h_3 decays.

The paper is organized as follows: we begin by presenting a theoretical setup of the C2HDM in section 2, especially focused on the mass and decays of h_3 ; then, after discussing in section 3 the software and the simulation procedure used, we present our results in section 4. We finish the paper with some conclusions in section 5.

2 Theoretical setup

2.1 The model at tree-level

Details on the Type II C2HDM and its renormalization can be found in refs. [24,25]. Here, we summarize the most relevant aspects for the analysis of the mass and decays of h_3 . We write the potential as:

$$V = m_{11}^2 |\Phi_1|^2 + m_{22}^2 |\Phi_2|^2 - \left(m_{12}^2 \Phi_1^\dagger \Phi_2 + \text{h.c.} \right) + \frac{\lambda_1}{2} (\Phi_1^\dagger \Phi_1)^2 + \frac{\lambda_2}{2} (\Phi_2^\dagger \Phi_2)^2 + \lambda_3 (\Phi_1^\dagger \Phi_1) (\Phi_2^\dagger \Phi_2) + \lambda_4 (\Phi_1^\dagger \Phi_2) (\Phi_2^\dagger \Phi_1) + \left[\frac{\lambda_5}{2} (\Phi_1^\dagger \Phi_2)^2 + \text{h.c.} \right]. \quad (1)$$

All parameters are forced to be real by hermiticity, except m_{12}^2 and λ_5 , which are in general complex. Φ_1 and Φ_2 are the scalar doublets, which we parameterize as:

$$\Phi_1 = \begin{pmatrix} \phi_1^+ \\ \frac{1}{\sqrt{2}}(v_1 e^{i\zeta_1} + \rho_1 + i\eta_1) \end{pmatrix}, \quad \Phi_2 = \begin{pmatrix} \phi_2^+ \\ \frac{1}{\sqrt{2}}(v_2 e^{i\zeta_2} + \rho_2 + i\eta_2) \end{pmatrix}, \quad (2)$$

where v_i are the real vacuum expectation values (vevs), ζ_i (real) phases, ρ_i and η_i real fields and ϕ_i^+ complex fields ($i = \{1, 2\}$). We introduce the total vev v and the angle β obeying the relations:

$$v^2 \equiv v_1^2 + v_2^2, \quad \tan(\beta) \equiv \frac{v_2}{v_1}. \quad (3)$$

Since there is CP violation at tree-level in the scalar sector, the fields ρ_i and η_i in eq. 2 will all mix at loop-level. To account for such mixing, one must consider the most general diagonalization at tree-level. We thus introduce the orthogonal matrix Q , such that:

$$S_n = Q \phi_n \quad \Leftrightarrow \quad \begin{pmatrix} h_1 \\ h_2 \\ h_3 \\ G_0 \end{pmatrix} = Q \begin{pmatrix} \rho_1 \\ \rho_2 \\ \eta_1 \\ \eta_2 \end{pmatrix}, \quad (4)$$

where G_0 is the would-be Goldstone boson, and h_1 , h_2 and h_3 are the physical neutral scalar bosons of the model, with masses m_1 , m_2 and m_3 , respectively, complying to $m_1 < m_2 < m_3$. The matrix Q is parameterized by six angles— $\alpha_0, \alpha_1, \alpha_2, \alpha_3, \alpha_4, \alpha_5$ —, according to:

$$Q = Q_5 Q_4 Q_3 Q_2 Q_1 Q_0, \quad (5)$$

with

$$\begin{aligned} Q_5 &= \begin{pmatrix} 1 & 0 & 0 & 0 \\ 0 & c_5 & 0 & s_5 \\ 0 & 0 & 1 & 0 \\ 0 & -s_5 & 0 & c_5 \end{pmatrix}, \quad Q_4 = \begin{pmatrix} c_4 & 0 & 0 & s_4 \\ 0 & 1 & 0 & 0 \\ 0 & 0 & 1 & 0 \\ -s_4 & 0 & 0 & c_4 \end{pmatrix}, \quad Q_3 = \begin{pmatrix} 1 & 0 & 0 & 0 \\ 0 & c_3 & s_3 & 0 \\ 0 & -s_3 & c_3 & 0 \\ 0 & 0 & 0 & 1 \end{pmatrix}, \\ Q_2 &= \begin{pmatrix} c_2 & 0 & s_2 & 0 \\ 0 & 1 & 0 & 0 \\ -s_2 & 0 & c_2 & 0 \\ 0 & 0 & 0 & 1 \end{pmatrix}, \quad Q_1 = \begin{pmatrix} c_1 & s_1 & 0 & 0 \\ -s_1 & c_1 & 0 & 0 \\ 0 & 0 & 1 & 0 \\ 0 & 0 & 0 & 1 \end{pmatrix}, \quad Q_0 = \begin{pmatrix} 1 & 0 & 0 & 0 \\ 0 & 1 & 0 & 0 \\ 0 & 0 & -s_0 & c_0 \\ 0 & 0 & c_0 & s_0 \end{pmatrix}, \end{aligned} \quad (6)$$

with $s_i = \sin \alpha_i$, $c_i = \cos \alpha_i$ ($i = \{0, 1, 2, 3, 4, 5\}$). The charged scalars in the mass basis, G^+ and H^+ (with G^+ being the charged would-be Goldstone boson), can be defined in a similar fashion. It turns out that, among the parameters just introduced, several of them end up being dependent, in such a way that several combinations of dependent parameters can be chosen. Following ref. [24], we focus on the four combinations displayed in table 1. In each combination C_i ($i = \{1, 2, 3, 4\}$), m_3^2 is a dependent parameter, and is hence fixed as a function of the independent parameters of the combination at stake.¹

Combination	Dependent parameters			
C_1	m_3^2 ,	ζ_1 ,	α_0 ,	α_4
C_2	m_3^2 ,	ζ_1 ,	α_0 ,	α_5
C_3	m_3^2 ,	ζ_1 ,	α_4 ,	α_5
C_4	m_3^2 ,	α_0 ,	α_4 ,	α_5

Table 1: Dependent parameters for each combination C_i .

2.2 The mass of h_3

When the C2HDM is considered not simply at tree-level—or at leading order (LO)—, but up to one-loop level—or at next-to-leading order (NLO)—, the original quantities of the model (parameters and fields) are taken to be bare quantities. These are shown in the following with index “(0)” and are separated into renormalized quantities and counterterms; for example, for the squared mass of h_3 ,

$$m_{3(0)}^2 = m_{3R}^2 + \delta m_3^2. \quad (7)$$

In this relation, and contrary to what we do for most of the remaining parameters, the renormalized squared mass m_{3R}^2 explicitly includes an index R. The reason is that, as we saw, the squared mass of h_3 was chosen as a dependent parameter, which means that $m_{3(0)}^2$ is also dependent, which in turn implies

¹The expressions for m_3^2 in the different combinations are very cumbersome, so that we omit them here.

that both m_{3R}^2 and δm_3^2 are also dependent, i.e. fixed.² As a consequence, m_{3R}^2 cannot be set equal to the squared pole mass of h_3 , which we identify with m_{3P}^2 . Up to one-loop level, the two masses are related by [24]:³

$$m_{3P}^2 = m_{3R}^2 - \widetilde{\text{Re}} \Sigma^{h_3 h_3}(m_{3R}^2) + \delta m_3^2, \quad (8)$$

where $\Sigma^{h_3 h_3}$ is the non-renormalized one-loop diagonal 2-point function of h_3 . Now, since the tree-level mass m_3 depended on the combination C_i (so that it was given by different expressions in the different combinations), the counterterm δm_3^2 will also correspond to different expressions according to the combination. More specifically, we can write⁴

$$\delta m_3^2 \stackrel{C_1}{=} \delta m_3^2(\delta m_1^2, \delta m_2^2, \delta\beta, \delta\alpha_1, \delta\alpha_2, \delta\alpha_3, \delta\alpha_5), \quad (9a)$$

$$\delta m_3^2 \stackrel{C_2}{=} \delta m_3^2(\delta m_1^2, \delta m_2^2, \delta\beta, \delta\alpha_1, \delta\alpha_2, \delta\alpha_3, \delta\alpha_4), \quad (9b)$$

$$\delta m_3^2 \stackrel{C_3}{=} \delta m_3^2(\delta m_1^2, \delta m_2^2, \delta\beta, \delta\alpha_1, \delta\alpha_2, \delta\alpha_3, \delta\alpha_0), \quad (9c)$$

$$\delta m_3^2 \stackrel{C_4}{=} \delta m_3^2(\delta m_1^2, \delta m_2^2, \delta\beta, \delta\alpha_1, \delta\alpha_2, \delta\alpha_3, \delta\zeta_1). \quad (9d)$$

The mass counterterms δm_1^2 and δm_2^2 are calculated in the on-shell subtraction (OSS) scheme. In the combination C_4 (where $\delta\zeta_1$ is independent), $\delta\zeta_1$ is calculated in the modified minimal subtraction ($\overline{\text{MS}}$) scheme; this will introduce an explicit dependence on the renormalization scale, μ_R . We fix the mixing parameters using symmetry relations [24]; this requires the introduction of the field counterterms for the scalar fields, according to:

$$\begin{pmatrix} G_{(0)}^+ \\ H_{(0)}^+ \end{pmatrix} = \begin{pmatrix} 1 + \frac{1}{2}\delta Z_{G^+ G^+} & \frac{1}{2}\delta Z_{G^+ H^+} \\ \frac{1}{2}\delta Z_{H^+ G^+} & 1 + \frac{1}{2}\delta Z_{H^+ H^+} \end{pmatrix} \begin{pmatrix} G^+ \\ H^+ \end{pmatrix}, \quad (10a)$$

$$\begin{pmatrix} h_{1(0)} \\ h_{2(0)} \\ h_{3(0)} \\ G_{0(0)} \end{pmatrix} = \begin{pmatrix} 1 + \frac{1}{2}\delta Z_{h_1 h_1} & \frac{1}{2}\delta Z_{h_1 h_2} & \frac{1}{2}\delta Z_{h_1 h_3} & \frac{1}{2}\delta Z_{h_1 G_0} \\ \frac{1}{2}\delta Z_{h_2 h_1} & 1 + \frac{1}{2}\delta Z_{h_2 h_2} & \frac{1}{2}\delta Z_{h_2 h_3} & \frac{1}{2}\delta Z_{h_2 G_0} \\ \frac{1}{2}\delta Z_{h_3 h_1} & \frac{1}{2}\delta Z_{h_3 h_2} & 1 + \frac{1}{2}\delta Z_{h_3 h_3} & \frac{1}{2}\delta Z_{h_3 G_0} \\ \frac{1}{2}\delta Z_{G_0 h_1} & \frac{1}{2}\delta Z_{G_0 h_2} & \frac{1}{2}\delta Z_{G_0 h_3} & 1 + \frac{1}{2}\delta Z_{G_0 G_0} \end{pmatrix} \begin{pmatrix} h_1 \\ h_2 \\ h_3 \\ G_0 \end{pmatrix}. \quad (10b)$$

All the field counterterms involved in these equations are fixed in the OSS scheme.⁵ Then, the relevant counterterms for the mixing parameters are defined as:

$$\delta\beta = \frac{1}{4} \text{Re} \left[\delta Z_{G^+ H^+} - \delta Z_{H^+ G^+} \right] \Big|_{\xi=1}, \quad (11a)$$

$$\delta\alpha_0 \stackrel{C_3}{=} \frac{1}{4} \sec(\alpha_2) \sec(\alpha_3) (\delta Z_{G_0 h_3} - \delta Z_{h_3 G_0}) \Big|_{\xi=1}, \quad (11b)$$

$$\delta\alpha_1 = \frac{1}{4} \sec(\alpha_2) \left[\cos(\alpha_3) (\delta Z_{h_1 h_2} - \delta Z_{h_2 h_1}) + \sin(\alpha_3) (\delta Z_{h_3 h_1} - \delta Z_{h_1 h_3}) \right] \Big|_{\xi=1}, \quad (11c)$$

²Finite parts can in principle be freely chosen; however, we will want m_{3R}^2 to correspond to the expression for the mass of h_3 which is obtained when the C2HDM is studied solely at tree-level (i.e. without aiming at the renormalization of the theory) [21], so that we exclude such freedom.

³We use the definition of real pole mass, also known as Breit-Wigner mass. The operator $\widetilde{\text{Re}}$, which is commonly used in the on-shell subtraction scheme, neglects the imaginary parts of loop integrals, while keeping the imaginary parts of complex parameters.

⁴The notation $\stackrel{C_i}{=}$ means that the equality at stake is only valid for the combination C_i . Just as the expressions for m_3^2 are tree-level (recall note 1), the expression for δm_3^2 in the different combinations are extremely cumbersome; we omit them as well.

⁵As in ref. [24], we extend the original OSS scheme (which applies to physical particles only) to apply also to the would-be Goldstone bosons.

$$\delta\alpha_2 = \frac{1}{4} \sin(\alpha_3) \left[\delta Z_{h_1 h_2} - \delta Z_{h_2 h_1} + \cot(\alpha_3) (\delta Z_{h_1 h_3} - \delta Z_{h_3 h_1}) \right] \Big|_{\xi=1}, \quad (11d)$$

$$\delta\alpha_3 = \frac{1}{4} \left[\delta Z_{h_2 h_3} - \delta Z_{h_3 h_2} - \cos(\alpha_3) \tan(\alpha_2) (\delta Z_{h_1 h_2} - \delta Z_{h_2 h_1}) + \sin(\alpha_3) \tan(\alpha_2) (\delta Z_{h_1 h_3} - \delta Z_{h_3 h_1}) \right] \Big|_{\xi=1}, \quad (11e)$$

$$\delta\alpha_4 \stackrel{C_2}{=} \frac{1}{4} \left[\delta Z_{h_1 G_0} - \delta Z_{G_0 h_1} + \sec(\alpha_3) \tan(\alpha_2) (\delta Z_{G_0 h_3} - \delta Z_{h_3 G_0}) \right] \Big|_{\xi=1}, \quad (11f)$$

$$\delta\alpha_5 \stackrel{C_1}{=} \frac{1}{4} \left[\delta Z_{h_2 G_0} - \delta Z_{G_0 h_2} + \tan(\alpha_3) (\delta Z_{G_0 h_3} - \delta Z_{h_3 G_0}) \right] \Big|_{\xi=1}, \quad (11g)$$

where $|_{\xi=1}$ means that the calculation is performed in the Feynman gauge.⁶ In this way, and given eqs. 9, it is clear that δm_3^2 depends on the combination C_i .

Such dependence on the combinations is *not* verified for m_{3R}^2 , as we now clarify. The different combinations were introduced because we considered a multiplicity of parameters at tree-level (as in eq. 6). This multiplicity was needed in order to generate all the countertterms required to absorb the one-loop divergences (as in eq. 11). Now, once the counterterms are generated—by separating the original parameters into renormalized ones and counterterms—the renormalized parameters are generated as well, and in the same quantity as the counterterms. However, several renormalized parameters can be absorbed away; in fact, since their bare versions were considered with the single purpose of yielding counterterms—and in such a way that, were it not for the counterterms, a small set could have been introduced—a simpler parameterization can be used for the renormalized parameters.⁷ More specifically, the renormalized parameters obey:

$$\zeta_{1R} = \alpha_4 = \alpha_5 = 0, \quad \alpha_0 = \beta. \quad (12)$$

This means, finally, that the renormalized parameters do not depend on combinations. In particular, whichever the combination C_i chosen, the renormalized squared mass of h_3 reads:

$$m_{3R}^2 = \frac{m_1^2 R_{13}(R_{12} \tan \beta - R_{11}) + m_2^2 R_{23}(R_{22} \tan \beta - R_{21})}{R_{33}(R_{31} - R_{32} \tan \beta)}, \quad (13)$$

where the matrix R is given by:

$$R = \begin{pmatrix} c_1 c_2 & s_1 c_2 & s_2 \\ -(c_1 s_2 s_3 + s_1 c_3) & c_1 c_3 - s_1 s_2 s_3 & c_2 s_3 \\ -c_1 s_2 c_3 + s_1 s_3 & -(c_1 s_3 + s_1 s_2 c_3) & c_2 c_3 \end{pmatrix}. \quad (14)$$

We will be interested in studying the relative corrections to the mass of h_3 , defined as:

$$\Delta m_3 \equiv \frac{m_{3P} - m_{3R}}{m_{3R}}. \quad (15)$$

Note that this quantity depends on the combination C_i , since m_{3P} depends on C_i (through δm_3^2 , recall eq. 8).

⁶These counterterms are *defined* in this gauge. Hence, even if the calculation of the S -matrix is performed in a different gauge (which implies that the remaining counterterms and the non-renormalized functions are calculated in that gauge), the counterterms in eqs. 11 are nonetheless calculated in the Feynman gauge. In the end, the S -matrix elements are ensured to be gauge independent. For details, see ref. [24].

⁷More details can be found in ref. [24]. Following this reference, we write the renormalized phase ζ_{1R} with an explicit R subscript (see also ref. [25]).

2.3 NLO decay widths of h_3

We now focus on decays of h_3 . If j represents the process corresponding to a certain decay of h_3 , the renormalized NLO amplitude for j can be written as:

$$\hat{\mathcal{M}}_j = \mathcal{M}_j^{\text{tree}} + \hat{\mathcal{M}}_j^{\text{loop}} = \mathcal{M}_j^{\text{tree}} + \mathcal{M}_j^{\text{loop}} + \mathcal{M}_j^{\text{CT}}. \quad (16)$$

Here, $\mathcal{M}_j^{\text{tree}}$ represents the tree-level (or LO) amplitude, $\hat{\mathcal{M}}_j^{\text{loop}}$ the renormalized one-loop amplitude, $\mathcal{M}_j^{\text{loop}}$ the non-renormalized one-loop amplitude and $\mathcal{M}_j^{\text{CT}}$ the total counterterm. The latter includes all the individual counterterms that end up contributing to the process j . Since different combinations of counterterms are taken as independent in the four C_i —in such a way that certain counterterms (like $\delta\alpha_0$) have different expressions in the different combinations—, $\mathcal{M}_j^{\text{CT}}$ takes different values in the different combinations. In this way, $\hat{\mathcal{M}}_j$ depends on the combination C_i .

Once $\hat{\mathcal{M}}_j$ is calculated, one can determine the NLO decay width, Γ_j^{NLO} . It is convenient to split the latter into three components:

$$\Gamma_j^{\text{NLO}} = \Gamma_j^{\text{LO}} + \Gamma_j^{\text{mix}} + \Gamma_j^{m_3}. \quad (17)$$

On the right-hand side, the first term configures the pure LO contribution, the second one represents the mixing between the tree-level and the renormalized one-loop contributions, and the last one represents the contributions to the NLO decay width arising from the corrections to the mass of h_3 . The latter can be justified as follows. In the calculation of the decay width of j , there will be occurrences of the momentum squared of h_3 . In principle, for an on-shell h_3 , such quantity corresponds to the physical mass of h_3 squared, $m_{3\text{P}}^2$. However, such identification would already contain corrections to a leading-order prediction, since $m_{3\text{P}}^2$ includes NLO effects. Therefore, we calculate Γ_j^{LO} and Γ_j^{mix} assuming that the momentum squared of h_3 is $m_{3\text{R}}^2$, and we define $\Gamma_j^{m_3}$ as the NLO effects that show up when one calculates Γ_j^{LO} by associating the momentum squared of h_3 to $m_{3\text{P}}^2$.⁸

In what follows, we consider four different decays of h_3 : to ZZ , h_1Z , h_2Z and h_2h_1 . For each of them, we write not only $\mathcal{M}_j^{\text{tree}}$ and $\hat{\mathcal{M}}_j^{\text{loop}}$ in terms of form factors, but also the three components of the right-hand side of eq. 17.⁹

2.3.1 $h_3 \rightarrow ZZ$

For $h_3 \rightarrow ZZ$, we define the momenta and Lorentz indices such that $h_3(p_1) \rightarrow Z^\nu(q_1)Z^\sigma(q_2)$, so that:

$$\mathcal{M}_{h_3 \rightarrow ZZ}^{\text{tree}} = \varepsilon_\nu^*(q_1) \varepsilon_\sigma^*(q_2) f_{ZZ,3}^{\text{tree}} g^{\nu\sigma}, \quad (18a)$$

⁸More precisely, $\Gamma_j^{m_3}$ is calculated by replacing all occurrences of $m_{3\text{R}}$ in Γ_j^{LO} by $m_{3\text{R}}$ plus the NLO correction to this mass, and expanding in series to first order in the NLO correction. In this way, we avoid including several beyond-NLO effects that would show up through the cavalier replacement of $m_{3\text{R}}$ by $m_{3\text{P}}$. It should be clear, however, that the definition of the pole mass in eq. 8 already ignores beyond-NLO effects. It can be argued that such effects may also be ignored in the calculation of the decay width; this is the usual procedure in the Minimal Supersymmetric Standard Model (cf. e.g. [33–37]). Here, by calculating $\Gamma_j^{m_3}$ the way we do, not only do we obtain a more strict NLO calculation, but we also distinguish the NLO contributions arising from the corrections to the mass ($\Gamma_j^{m_3}$) from those arising from the corrections to the vertex (Γ_j^{mix}).

⁹The form factors are identified by the letter f , containing a subscript which starts with the particles in the final state, followed by a natural number. The attribution of natural numbers follows the conventions of FEYNMASTER [24, 38], which do not exploit momentum conservation. Tree-level form factors are identified with the superscript ‘tree’. We omit the expressions corresponding to the form factors, which are in general extremely large.

$$\hat{\mathcal{M}}_{h_3 \rightarrow ZZ}^{\text{loop}} = \varepsilon_\nu^*(q_1) \varepsilon_\sigma^*(q_2) \left(f_{ZZ,3} g^{\nu\sigma} + f_{ZZ,6} p_1^\nu p_1^\sigma + f_{ZZ,9} p_1^\nu q_1^\sigma + f_{ZZ,24} p_1^\sigma q_2^\nu + f_{ZZ,27} q_1^\sigma q_2^\nu \right. \\ \left. + f_{ZZ,33} p_1^\omega q_1^\nu \epsilon^{\nu\sigma\omega\nu} + f_{ZZ,15} p_1^\sigma q_1^\nu + f_{ZZ,18} q_1^\nu q_1^\sigma + f_{ZZ,21} q_1^\nu q_2^\sigma \right). \quad (18b)$$

As a consequence,

$$\Gamma_{h_3 \rightarrow ZZ}^{\text{LO}} = \frac{\sqrt{m_{3R}^4 - 4 m_{3R}^2 m_Z^2}}{128 \pi m_{3R}^3 m_Z^4} (m_{3R}^4 - 4 m_{3R}^2 m_Z^2 + 12 m_Z^4) (f_3^{\text{tree}})^2, \quad (19a)$$

$$\Gamma_{h_3 \rightarrow ZZ}^{\text{mix}} = \frac{\sqrt{m_{3R}^4 - 4 m_{3R}^2 m_Z^2}}{128 \pi m_{3R}^3 m_Z^4} f_3^{\text{tree}} \left\{ 2 (m_{3R}^4 - 4 m_{3R}^2 m_Z^2 + 12 m_Z^4) \text{Re}[f_3] \right. \\ \left. + m_{3R}^2 (m_{3R}^4 - 6 m_{3R}^2 m_Z^2 + 8 m_Z^4) \text{Re}[f_{ZZ,6} + f_{ZZ,9} + f_{ZZ,24} + f_{ZZ,27}] \right\}, \quad (19b)$$

$$\Gamma_{h_3 \rightarrow ZZ}^{m_3} = 3 \Delta m_3 \Gamma_{h_3 \rightarrow ZZ}^{\text{LO}} \frac{m_{3R}^6 - 4 m_{3R}^4 m_Z^2 - 4 m_{3R}^2 m_Z^4 + 32 m_Z^6}{m_{3R}^6 - 8 m_{3R}^4 m_Z^2 + 28 m_{3R}^2 m_Z^4 - 48 m_Z^6}. \quad (19c)$$

2.3.2 $h_3 \rightarrow h_1 Z$

Concerning the decay $h_3 \rightarrow h_1 Z$, we define the momenta and Lorentz indices such that $h_3(p_1) \rightarrow h_1(q_1) Z^\sigma(q_2)$, and we define form factors such that:

$$\mathcal{M}_{h_3 \rightarrow h_1 Z}^{\text{tree}} = \varepsilon_\sigma^*(q_2) (f_{1Z,3}^{\text{tree}} q_1^\sigma + f_{1Z,9}^{\text{tree}} p_1^\sigma), \quad \hat{\mathcal{M}}_{h_3 \rightarrow h_1 Z}^{\text{loop}} = \varepsilon_\sigma^*(q_2) (f_{1Z,3} q_1^\sigma + f_{1Z,6} q_2^\sigma + f_{1Z,9} p_1^\sigma). \quad (20)$$

Then, we have:

$$\Gamma_{h_3 \rightarrow h_1 Z}^{\text{LO}} = \frac{|f_{1Z,3}^{\text{tree}} + f_{1Z,9}^{\text{tree}}|^2}{64 \pi m_{3R}^3 m_Z^2} \left(m_{3R}^4 + m_1^4 + m_Z^4 - 2 m_{3R}^2 m_1^2 - 2 m_{3R}^2 m_Z^2 - 2 m_1^2 m_Z^2 \right)^{3/2}, \quad (21a)$$

$$\Gamma_{h_3 \rightarrow h_1 Z}^{\text{mix}} = \frac{\text{Re} [(f_{1Z,3}^{\text{tree}} + f_{1Z,9}^{\text{tree}}) (f_{1Z,3}^* + f_{1Z,9}^*)]}{32 \pi m_{3R}^3 m_Z^2} \left(m_{3R}^4 + m_1^4 + m_Z^4 - 2 m_{3R}^2 m_1^2 - 2 m_{3R}^2 m_Z^2 - 2 m_1^2 m_Z^2 \right)^{3/2}, \quad (21b)$$

$$\Gamma_{h_3 \rightarrow h_1 Z}^{m_3} = -3 \Delta m_3 \Gamma_{h_3 \rightarrow h_1 Z}^{\text{LO}} \frac{m_1^4 - m_{3R}^4 - 2 m_1^2 m_Z^2 + m_Z^4}{m_{3R}^4 + m_1^4 + m_Z^4 - 2 m_{3R}^2 m_1^2 - 2 m_{3R}^2 m_Z^2 - 2 m_1^2 m_Z^2}. \quad (21c)$$

2.3.3 $h_3 \rightarrow h_2 Z$

Similarly for $h_3 \rightarrow h_2 Z$, we define the momenta and Lorentz indices such that $h_3(p_1) \rightarrow h_2(q_1) Z^\sigma(q_2)$, and we define form factors such that:

$$\mathcal{M}_{h_3 \rightarrow h_2 Z}^{\text{tree}} = \varepsilon_\sigma^*(q_2) (f_{2Z,3}^{\text{tree}} q_1^\sigma + f_{2Z,9}^{\text{tree}} p_1^\sigma), \quad \hat{\mathcal{M}}_{h_3 \rightarrow h_2 Z}^{\text{loop}} = \varepsilon_\sigma^*(q_2) (f_{2Z,3} q_1^\sigma + f_{2Z,6} q_2^\sigma + f_{2Z,9} p_1^\sigma). \quad (22)$$

Then,

$$\Gamma_{h_3 \rightarrow h_2 Z}^{\text{LO}} = \frac{|f_{2Z,3}^{\text{tree}} + f_{2Z,9}^{\text{tree}}|^2}{64 \pi m_{3R}^3 m_Z^2} \left(m_{3R}^4 + m_2^4 + m_Z^4 - 2 m_{3R}^2 m_2^2 - 2 m_{3R}^2 m_Z^2 - 2 m_2^2 m_Z^2 \right)^{3/2}, \quad (23a)$$

$$\Gamma_{h_3 \rightarrow h_2 Z}^{\text{mix}} = \frac{\text{Re} [(f_{2Z,3}^{\text{tree}} + f_{2Z,9}^{\text{tree}}) (f_{2Z,3}^* + f_{2Z,9}^*)]}{32 \pi m_{3R}^3 m_Z^2} \left(m_{3R}^4 + m_2^4 + m_Z^4 - 2 m_{3R}^2 m_2^2 - 2 m_{3R}^2 m_Z^2 - 2 m_2^2 m_Z^2 \right)^{3/2}, \quad (23b)$$

$$\Gamma_{h_3 \rightarrow h_2 Z}^{m_3} = -3 \Delta m_3 \Gamma_{h_3 \rightarrow h_2 Z}^{\text{LO}} \frac{m_2^4 - m_{3R}^4 - 2 m_2^2 m_Z^2 + m_Z^4}{m_{3R}^4 + m_2^4 + m_Z^4 - 2 m_{3R}^2 m_2^2 - 2 m_{3R}^2 m_Z^2 - 2 m_2^2 m_Z^2}. \quad (23c)$$

2.3.4 $h_3 \rightarrow h_2 h_1$

In this case, we simply have:

$$\hat{\mathcal{M}}_{h_3 \rightarrow h_2 h_1} = \mathcal{M}_{h_3 \rightarrow h_2 h_1}^{\text{tree}} + \hat{\mathcal{M}}_{h_3 \rightarrow h_2 h_1}^{\text{loop}} = f_{21,1}^{\text{tree}} + f_{21,1}, \quad (24)$$

so that:

$$\Gamma_{h_3 \rightarrow h_2 h_1}^{\text{LO}} = \frac{\sqrt{m_{3R}^4 + m_1^4 + m_2^4 - 2m_{3R}^2 m_1^2 - 2m_{3R}^2 m_2^2 - 2m_1^2 m_2^2}}{16 \pi m_{3R}^3} (f_{21,1}^{\text{tree}})^2, \quad (25a)$$

$$\Gamma_{h_3 \rightarrow h_2 h_1}^{\text{mix}} = \frac{\sqrt{m_{3R}^4 + m_1^4 + m_2^4 - 2m_{3R}^2 m_1^2 - 2m_{3R}^2 m_2^2 - 2m_1^2 m_2^2}}{8 \pi m_{3R}^3} f_{21,1}^{\text{tree}} \text{Re}[f_{21,1}], \quad (25b)$$

$$\Gamma_{h_3 \rightarrow h_2 h_1}^{m_3} = -\Delta m_3 \Gamma_{h_3 \rightarrow h_2 h_1}^{\text{LO}} \frac{3(m_1^2 - m_2^2)^2 - 4(m_1^2 + m_2^2)m_{3R}^2 + m_{3R}^4}{m_{3R}^4 + m_1^4 + m_2^4 - 2m_{3R}^2 m_1^2 - 2m_{3R}^2 m_2^2 - 2m_1^2 m_2^2}. \quad (25c)$$

3 Computational tools and simulation procedure

The Feynman rules, counterterms, one-loop amplitudes and decay widths were all calculated with FEYNMASTER [24, 38], which resorts to FEYNRULES [39, 40], QGRAF [41] and FEYNCALC [42–44]. FEYNMASTER was also used to convert the results to FORTRAN, where they were numerically evaluated using LOOPTOOLS [45]. For the scatter plots that follow, we generated points in the parameter space of the Type II C2HDM; we identified h_1 with the SM-like Higgs boson, implying $m_1 = 125$ GeV. We restricted the parameter space by considering both theoretical and experimental constraints. The former consist of perturbative unitarity [46, 47], boundeness from below [48], the requirement of vacuum globality [49] and the restrictions concerning the oblique parameters S, T, U [5]. Regarding the experimental constraints, we demanded a 2σ compatibility with the results coming from both $B \rightarrow X_s \gamma$ [50–54] and R_b [50, 55]; besides, signals for the SM-like Higgs boson were taken into account by requiring points to be compatible with the fits put forward in ref. [56], whereas exclusion bounds coming from searches of extra Higgs bosons were included via HIGGSBOUNDS5 [57]. The most severe current limit on the electric dipole moment (EDM) of the electron, $|d_e| < 1.1 \times 10^{-29} e \text{ cm}$ at 90% confidence level, provided by the ACME collaboration [58], was also employed. Finally, we choose as input parameters of the potential the set:

$$\{p^V\} = \{\alpha_1, \alpha_2, \alpha_3, \beta, m_1, m_2, m_{H^+}, \text{Re } m_{12}^2\}, \quad (26)$$

where m_{H^+} is the mass of H^+ , and we vary them according to:

$$\begin{aligned} -\frac{\pi}{2} \leq \alpha_{1,2,3} < \frac{\pi}{2}, \quad 1 \leq \tan \beta \leq 10, \quad 30 \text{ GeV} \leq m_2 < 800 \text{ GeV}, \\ 580 \text{ GeV} \leq m_{H^\pm} < 800 \text{ GeV}, \quad 0 \text{ GeV}^2 \leq \text{Re } m_{12}^2 < 500000 \text{ GeV}^2. \end{aligned} \quad (27)$$

We generate and use three data sets, which optimize Γ_j^{LO} for $j = h_3 \rightarrow ZZ, h_3 \rightarrow h_1 Z$ and $h_3 \rightarrow h_2 Z$, respectively.¹⁰ This separation is relevant, since different regions of parameter space lead to non-negligible values of Γ_j^{LO} according to the decay j , as shall be discussed in the following section.

¹⁰Concerning $h_3 \rightarrow h_2 h_1$, see discussion in section 4.2.4.

4 Results and discussion

4.1 The mass of h_3

We start by investigating Δm_3 (defined in eq. 15) in each of the four combinations C_i .¹¹ The results are shown in figure 1, as a function of the renormalized mass. All the points coming from the three data sets mentioned in the last section are superimposed in the figure. It is clear that the four combinations

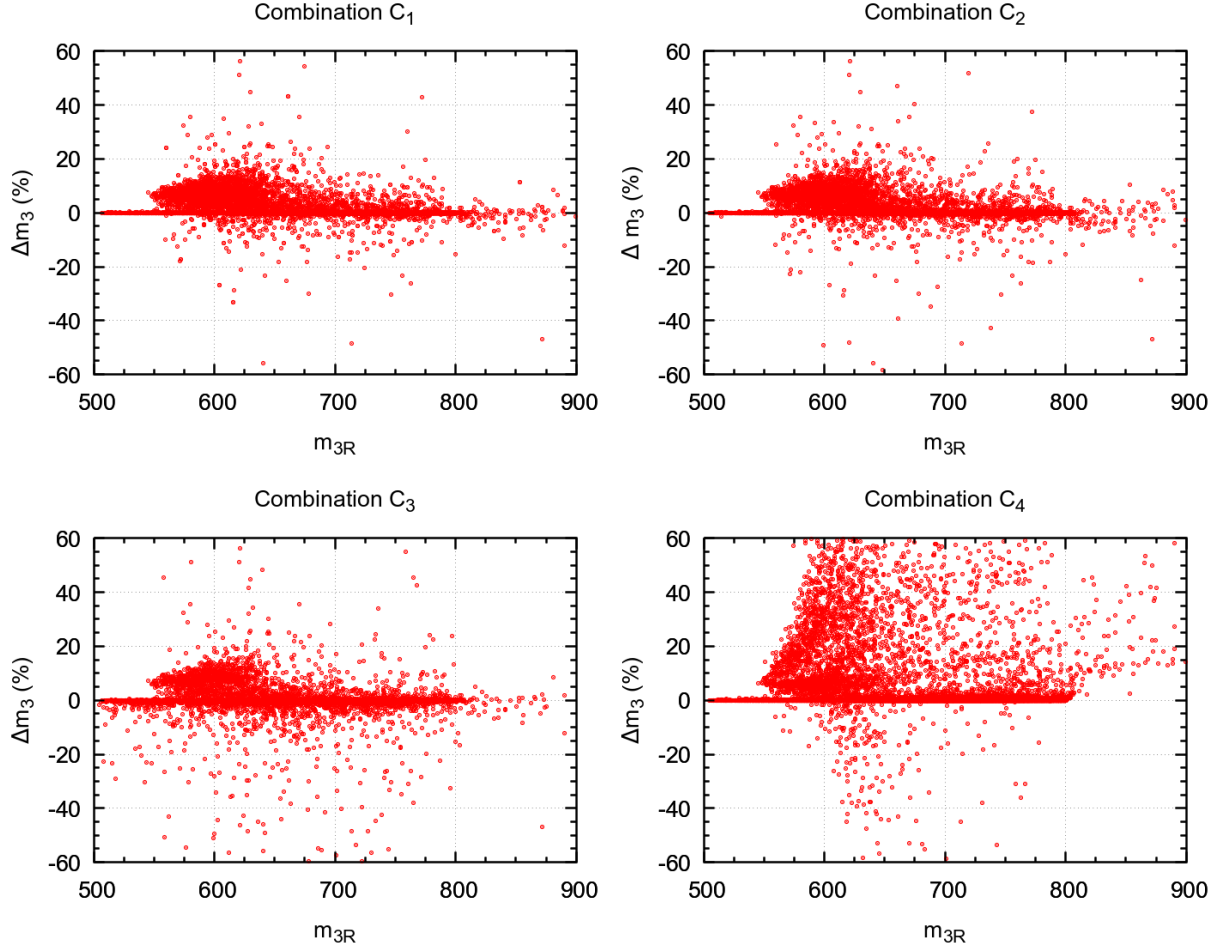


Figure 1: The quantity Δm_3 defined in eq. 15 for the different combinations: C_1 (top left), C_2 (top right), C_3 (bottom left) and C_4 with $\mu_R = 350$ GeV (bottom right). Only the range $-60\% < \Delta m_3 < 60\%$ is shown.

contain points which describe very large corrections. The reason can be traced back to δm_3^2 , which contributes to m_{3P} (and thus to Δm_3) according to eq. 8. As it turns out, δm_3^2 takes very large values in all combinations for very specific regions of the parameter space. To understand this aspect, notice that eq. 13 can be rewritten as:

$$m_{3R}^2 = \frac{m_1^2 \epsilon_1 + m_2^2 \epsilon_2}{(-\epsilon_3)}, \quad (28)$$

where we define

$$\epsilon_k \equiv R_{k3} (R_{k2} \tan \beta - R_{k1}), \quad (29)$$

¹¹As mentioned above, the combination C_4 has an explicit dependence on the renormalization scale, μ_R . In ref. [24], we studied three different scales for different processes calculated in C_4 , and concluded that $\mu_R = 350$ GeV led to the most well-behaved results. In what follows, we also use this scale.

where $k = \{1, 2, 3\}$ and where the matrix R is defined in eq. 14. We are interested in the case where ϵ_3 takes very small values, approaching zero. Since the expression for ϵ_3 is:

$$\epsilon_3 = c_2 c_3 \left\{ c_1 \left[s_2 c_3 - s_3 \tan(\beta) \right] - s_1 \left[s_2 c_3 \tan(\beta) + s_3 \right] \right\}, \quad (30)$$

we can distinguish two different scenarios—identified as S_1 and S_2 in the following—that lead to a vanishing ϵ_3 .¹²

$$S_1 : \alpha_3 = \pm \frac{\pi}{2}, \quad S_2 : \alpha_3 = \arctan \left[\cot(\alpha_1 + \beta) \sin(\alpha_2) \right]. \quad (31)$$

We thus see that, for α_3 close to either one or the other limit, m_{3R}^2 will tend to assume very large values, due to the smallness of the denominator ϵ_3 . There is, however, an exception: even if α_3 is close either to S_1 or S_2 , large values of m_{3R}^2 can be avoided if ϵ_1 and ϵ_2 are simultaneously small. In fact, if we happen to choose points in a very particular region of the parameter space where not only ϵ_3 , but also ϵ_1 and ϵ_2 approach zero, then the smallness of the latter (ϵ_1 and ϵ_2) compensates for the smallness of the former (ϵ_3), so that m_{3R}^2 ends up taking moderate values. Notice that *immoderate* values m_{3R}^2 would violate the theoretical constraints of the theory.¹³ As a consequence, if ϵ_3 is very small (through either S_1 or S_2), valid points can only be obtained if they are in the very fine-tuned region of parameter space which we alluded to (where both ϵ_1 and ϵ_2 approach zero) and which ensures that m_{3R}^2 is not very large.

It turns out that, in such particular region, there is a problem with the counterterm δm_3^2 , as we now explain. At tree-level, and like we saw at the end of section 2.1, the mass of h_3 is a derived parameter, which takes different (complicated) expressions in the different combinations. When we go up to one-loop level, each of those expressions (meanwhile identified as bare) generates a renormalized term and a counterterm, according to eq. 7. This happens in such a way that, as described in section 2.2, the renormalized term is given by eq. 13 in all the four combinations, whereas the counterterm δm_3^2 depends on the combination C_i . Now, for each combination, the expression for δm_3^2 is closely related to eq. 13, in the sense that both derive from the same original, bare expression. This suggests that, whenever eq. 13 tends to be very large, the values for the counterterm δm_3^2 in the different combinations will follow that trend. In particular, both scenarios described in eq. 31 will naturally lead to very large values of δm_3^2 . However, because the expressions for δm_3^2 are different from that of m_{3R}^2 (although related to it, as we saw), the very precise fine tuning that leads the latter to acquire a moderate value turns out not to be verified in the former. We thus end up with a peculiar situation: the points (not excluded by theoretical constraints) obeying the scenarios 31 require a very precise fine-tuning; this fine-tuning ensures that eq. 13 has moderate values (otherwise, the points would be excluded), but does *not* ensure that the expressions for δm_3^2 in the different combinations are also moderate. Hence, those points are valid points—since they pass all the constraints described in section 3—, but lead to very large values for the counterterm δm_3^2 in the different combinations.

In sum, there are points in very precise regions of the parameter space of the model that, although leading to acceptable values of m_{3R}^2 (due to a razor-sharp fine-tuning), generate very large values of

¹²In principle, $\alpha_2 = \pm \frac{\pi}{2}$ could also lead to a vanishing ϵ_3 . However, the theoretical constraints of the theory (in particular, those related to the electron EDM) force α_2 to take very small values.

¹³More specifically, they would violate the oblique parameter T.

the counterterm δm_3^2 ; the regions of parameter space at stake are those around the scenarios S_1 and S_2 described in eq. 31. Two notes are in order here. First, as we are about to see in detail, the precise regions at stake are indeed very precise (i.e. very fine-tuned), so that they are prone to be avoided by a random generation of points. Second, the immoderate values of δm_3^2 do *not* stem from an inappropriate choice of subtraction schemes. It does not happen, indeed, that the finite parts of the independent counterterms that δm_3^2 depends on become unusually large for the points at stake. Rather, the problem lies in the fact that the counterterms δm_3^2 in the different combinations correspond to complicated expressions involving quotients and trigonometrical functions, in such manner that those expressions diverge in certain particular limits of the renormalized parameters. The complicated character of the counterterms δm_3^2 , in turn, results from the circumstance that the bare parameter $m_{3(0)}^2$ depends in a complicated way on the independent parameters.¹⁴

In the following, we want to avoid points in the aforementioned very fine-tuned regions—i.e. points very near to either S_1 or S_2 . To better grasp the scenario S_2 , we ascertain in figure 2 the region of parameter space that it covers. In both panels, we represent in red a set of points optimized for the decay $h_3 \rightarrow ZZ$,

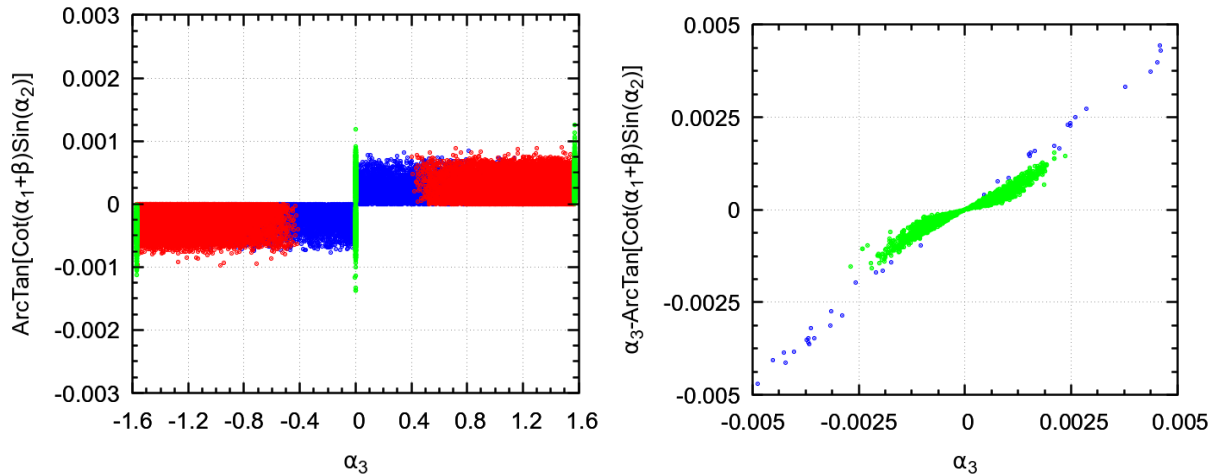


Figure 2: Left panel: $\arctan [\cot(\alpha_1 + \beta) \sin(\alpha_2)]$ against α_3 , for the whole range of α_3 . Right panel: the difference between α_3 and $\arctan [\cot(\alpha_1 + \beta) \sin(\alpha_2)]$ against α_3 , for a very restricted range of α_3 . In red, points leading to a non-negligible decay width for $h_3 \rightarrow ZZ$; in blue, points leading to a non-negligible decay width for $h_3 \rightarrow h_1 Z$; in green, points allowing the decay $h_3 \rightarrow h_2 Z$.

in blue a set of points optimized for the decay $h_3 \rightarrow h_1 Z$ and in green a set of points which allow the process $h_3 \rightarrow h_2 Z$ at tree-level (by complying to $m_{3R} > m_2 + m_Z$). From the red and the blue points on the left plot, it is clear that $\arctan [\cot(\alpha_1 + \beta) \sin(\alpha_2)]$ always takes very small values for the whole set of points; therefore, the scenario S_2 will be verified if and only if α_3 is very close to zero. This conclusion is also derived from the blue points on the right plot, where we show the difference between α_3 and $\arctan [\cot(\alpha_1 + \beta) \sin(\alpha_2)]$ against α_3 , for a very restricted range of the latter around zero. In sum: in order to avoid S_2 , points with $\alpha_3 \simeq 0$ must be avoided.

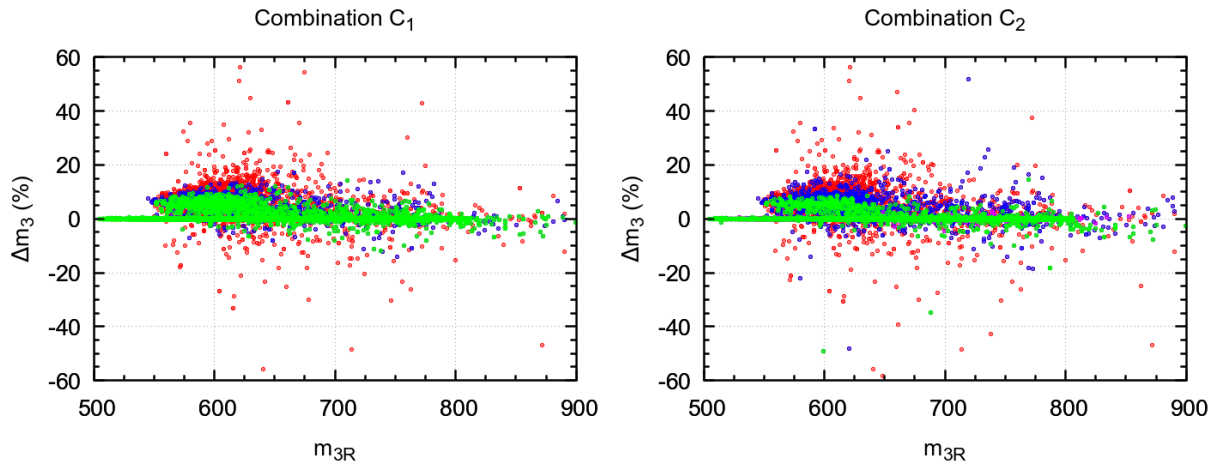
¹⁴One can argue that it is not really necessary to take the mass of h_3 as a dependent parameter of the C2HDM; indeed, although taking it as a dependent parameter is the most common option (see e.g. refs. [9, 12, 14, 15, 21]), one could also select one of the mixing angles instead [16, 19]. We follow here ref. [24], which proposed the renormalization of the model assuming the mass of h_3 as a derived parameter; the exploration of an alternative renormalization—where a mixing angle is taken as dependent instead of the mass of h_3 —is beyond the scope of this paper.

It is only after reaching such conclusion that we can properly appreciate the points represented in green. From the left plot, we see that those points (which, recall, are the ones enabling the decay $h_3 \rightarrow h_2 Z$) are restricted to very fine-tuned regions. More than just that: those very fine-tuned regions are *precisely* those around the troublesome scenarios S_1 and S_2 ; indeed, they are concentrated either around $\alpha_3 = \pm\pi/2$ (scenario S_1) or around $\alpha_3 = 0$ (scenario S_2). We can thus anticipate a tension which we will come back to in section 4.2.3 below: in the decay $h_3 \rightarrow h_2 Z$, since all the points allowing it are very close to either S_1 or S_2 , the values of δm_3^2 are generally very large, which in turn implies very large values of $\Gamma_{h_3 \rightarrow h_2 Z}^{\text{NLO}}$ (recall eqs. 8, 15, 17 and 23c). So, if one tries to avoid the regions S_1 and S_2 —in an attempt to obtain more stable results—, one is left with no points. In that decay, therefore, a compromise must be found: on the hand, one may wish to avoid the troublesome regions where δm_m^2 has a bad behaviour; on the other hand, one cannot significantly depart from those regions, for otherwise one ends up having no points. Notice that such compromise does exist in the decays $h_3 \rightarrow ZZ$ and $h_3 \rightarrow h_2 Z$, since one can find points which allow these processes and which are far away from both S_1 and S_2 .¹⁵

This difference between the processes—as well as the differences between the combinations—leads us to consider different types of cuts, in our attempt to avoid the troublesome regions S_1 and S_2 . This is illustrated in figure 3, where we show the same as in figure 1, but now including different cuts on the mixing angles. In all combinations, the points in blue correspond to cuts that shall be sufficient to generate adequate results for the decay $h_3 \rightarrow h_1 Z$, whereas the points in green correspond to cuts more adapted to $h_3 \rightarrow h_2 Z$.¹⁶ Some aspects should be highlighted here.

First, it is clear from all the plots that the more stringent the cuts, the smaller the range of Δm_3 . Or, which is the same, the more the scenarios S_1 and S_2 are avoided, the better the numerical stability of the corrections to the mass of h_3 . This proves that the numerical instabilities observed in the red points have to do with a proximity of the points to either S_1 or S_2 , so that the instabilities disappear when those scenarios are avoided.

Second, even after the cuts, we can still find points leading to large instabilities. This is especially



¹⁵The decay $h_3 \rightarrow h_2 h_1$ suffers from the same problem as $h_3 \rightarrow h_2 Z$, and will be considered in detail in section 4.2.4.

¹⁶As for the remaining processes discussed in this paper: $h_3 \rightarrow ZZ$ will require cuts less stringent than the ones represented in blue in figure 3, while $h_3 \rightarrow h_2 h_1$ will not have a sufficiently relevant branching ratio to justify a detailed analysis (for details, see section 4.2.4 below).

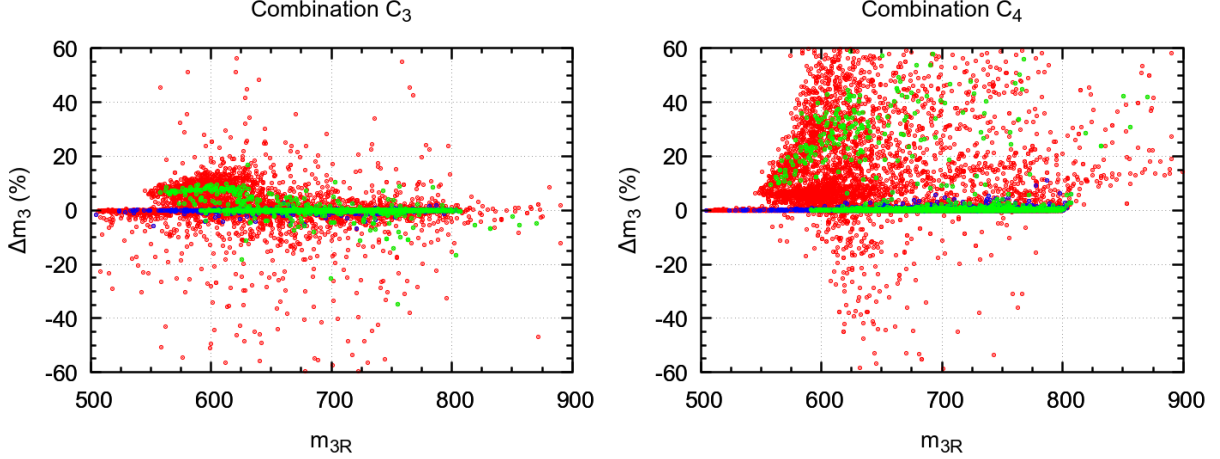


Figure 3: The same as in figure 1, but with extra cuts: in C_1 , blue points have $\pi/2 - |\alpha_3| > 0.0005$ and $|\alpha_3| > 0.0005$, whereas green points have $\pi/2 - |\alpha_3| > 0.0007$ and $|\alpha_3| > 0.00085$; in C_2 , blue points have $\pi/2 - |\alpha_3| > 0.0005$ and $|\alpha_3| > 0.0005$, whereas green points have $\pi/2 - |\alpha_3| > 0.00075$, $|\alpha_3| > 0.001075$ and $|\alpha_2| > 0.001$; in C_3 , blue points have $\pi/2 - |\alpha_3| > 0.005$, $|\alpha_3| > 0.05$ and $|\alpha_2| > 0.0025$, whereas green points have $\pi/2 - |\alpha_3| > 0.0004$, $|\alpha_3| > 0.005$ and $|\alpha_2| > 0.005$; C_4 is as C_3 .

true in the case of the blue points in the combination C_2 , where values as large as $\Delta m_3 \simeq 50\%$ can still be found. However, this is only because the cuts at stake are not sufficiently stringent; for example, in combination C_2 , the green points—which involve more severe cuts—lead to more stable results than the blue points.

Finally, the combination C_4 —which explicitly depends on the renormalization scale μ_R —is shown for $\mu_R = 350$ GeV. Yet, we found that the results strongly depend on the value of μ_R . For that reason, it will not be considered in what follows.

4.2 NLO decay widths of h_3

We now turn to the numerical results for the NLO decay widths. We want to investigate the importance of the NLO contributions. We thus define the relative correction to the decay width of j as:

$$\Delta\Gamma_j \equiv \frac{\Gamma_j^{\text{NLO}} - \Gamma_j^{\text{LO}}}{\Gamma_j^{\text{LO}}} = \frac{\Gamma_j^{\text{mix}} + \Gamma_j^{m_3}}{\Gamma_j^{\text{LO}}}, \quad (32)$$

where we used eq. 17. Notice that both Γ_j^{mix} and $\Gamma_j^{m_3}$ depend on the combination C_i ; the contribution coming from the former is expected to be *grasso modo* similar to that found in the decays of h_2 studied in ref. [24].¹⁷ Here, we are particularly interested in the contribution coming from $\Gamma_j^{m_3}$ (which was absent in decays of h_2 , since m_2 is an independent parameter). From the expressions presented in section 2.3.1 to 2.3.4, we see that, for every process j , a non-null difference between the pole mass and the renormalized mass of h_3 (i.e. $\Delta m_3 \neq 0$) leads to a non-null $\Gamma_j^{m_3}$.¹⁸ Actually, $\Gamma_j^{m_3}$ depends linearly on Δm_3 ; hence, the

¹⁷In fact, for a certain pair of final particles, the independent parameter counterterms are the same in the decays of h_2 and h_3 , and the field counterterms (which are different in the decays of h_2 and h_3) are all fixed through the same subtraction scheme; cf. ref. [24] for details.

¹⁸This happens despite the fact that there are no corrections coming from wave-function renormalization factors (also known as LSZ factors). Indeed, the circumstance that the field counterterms in eq. 10b were all fixed in the OSS scheme means that the wave-function renormalization factors become trivial [25]. Nonetheless, because the mass of h_3 is a derived parameter, there are in general contributions to the NLO decay width arising from their loop corrections, as explained in section 2.3.

larger is Δm_3 , the larger is $\Gamma_j^{m_3}$, and thus the larger is $\Delta\Gamma_j$. In face of this, we are now able to better grasp the consequences of the plots in figure 3; in fact, we realize that a large value of Δm_3 will generally imply large corrections for two types of observables: not only that corresponding to the physical mass of h_3 , but will to those corresponding to the decay widths of h_3 decays.

We now present results for the four decays described in section 2.3, following the same order.

4.2.1 $h_3 \rightarrow ZZ$

In figure 4, we show $\Delta\Gamma_{h_3 \rightarrow ZZ}$ in percentage against $\Gamma_{h_3 \rightarrow ZZ}^{\text{LO}}$ for the combinations C_1 , C_2 and C_3 . Whereas the red points represent the total correction, the green ones represent the contribution coming from $\Gamma_{h_3 \rightarrow ZZ}^{\text{mix}}$ and the blue ones the contribution coming from $\Gamma_{h_3 \rightarrow ZZ}^{m_3}$. We avoid the scenarios S_1 and S_2 by imposing the cuts described in the caption.

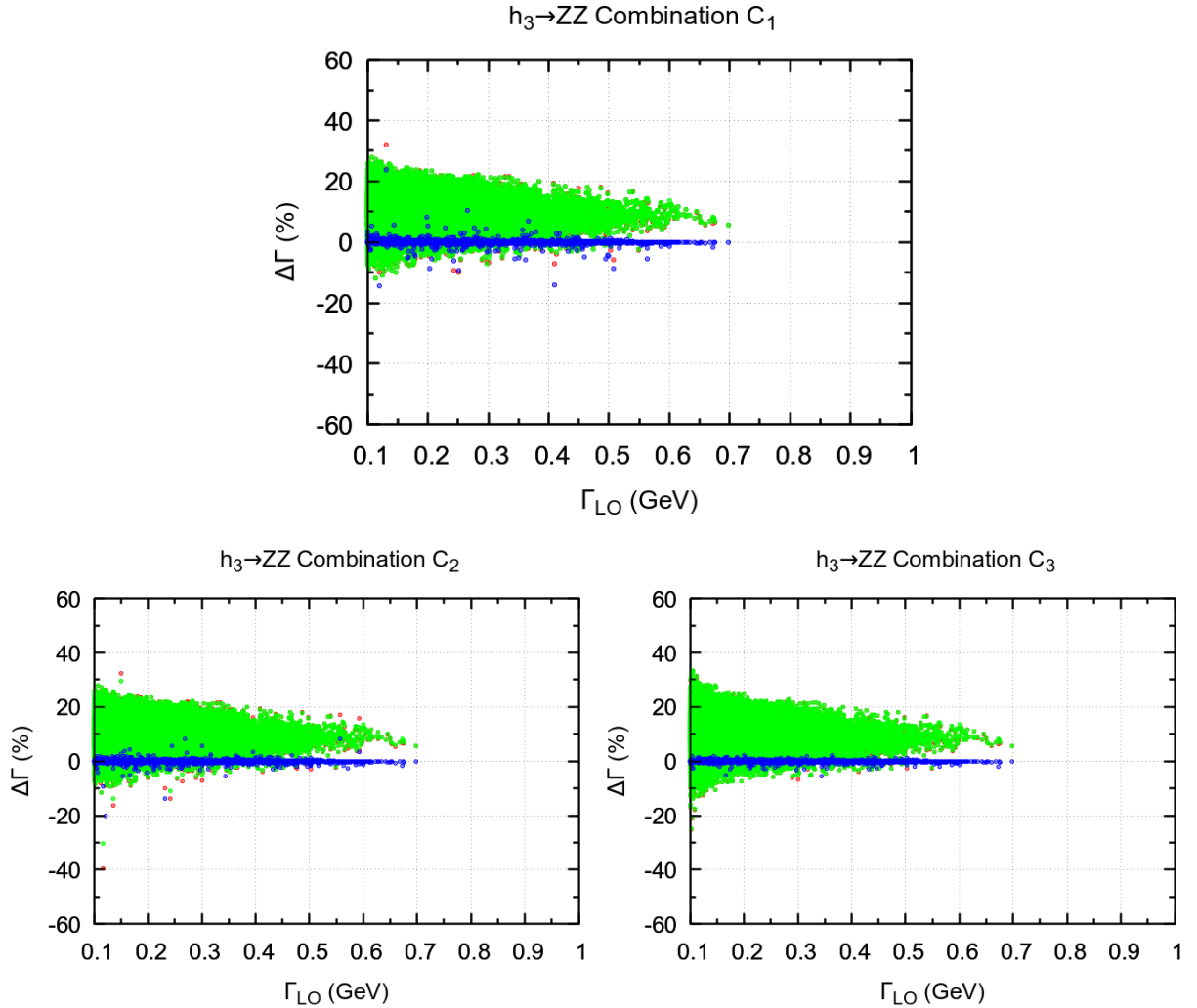


Figure 4: $\Delta\Gamma_{h_3 \rightarrow ZZ}$ in percentage against $\Gamma_{h_3 \rightarrow ZZ}^{\text{LO}}$, for the combinations C_1 (top), C_2 (bottom left) and C_3 (bottom right). For C_1 , we impose the cuts $\pi/2 - |\alpha_3| > 0.0005$ and $|\alpha_3| > 0$, whereas for C_2 and C_3 we impose the cuts $\pi/2 - |\alpha_3| > 0.005$ and $|\alpha_3| > 0$. Only the interval $0.1 \text{ GeV} < \Gamma_{h_3 \rightarrow ZZ}^{\text{LO}} < 1 \text{ GeV}$ is shown. In red, $\Delta\Gamma_{h_3 \rightarrow ZZ}$; in green, $\Gamma_{h_3 \rightarrow ZZ}^{\text{mix}}/\Gamma_{h_3 \rightarrow ZZ}^{\text{LO}}$; in blue, $\Gamma_{h_3 \rightarrow ZZ}^{m_3}/\Gamma_{h_3 \rightarrow ZZ}^{\text{LO}}$. According to eq. 32, the red points are the sum of the green and the blue ones.

It is clear that, in all the plots, smaller values of $\Gamma_{h_3 \rightarrow ZZ}^{\text{LO}}$ allow larger values of $\Delta\Gamma_{h_3 \rightarrow ZZ}$; the explanation

is simply that, as the denominator of 32 becomes smaller, the numerator does not necessarily mimic that reduction. Notice that whereas small values of $\Delta\Gamma_{h_3 \rightarrow ZZ}$ imply that a perturbative description of the theory is possible, large values would in principle require the calculation of the following order in perturbation theory, so as to ascertain the feasibility of such description.

As expected, the contribution arising from $\Gamma_{h_3 \rightarrow ZZ}^{\text{mix}}$ in all the plots is similar to the equivalent one in the decay $h_2 \rightarrow ZZ$, described in ref. [24]. Where the two processes differ is in the component $\Gamma_j^{m_3}$, which was absent in $h_2 \rightarrow ZZ$ but is present in $h_3 \rightarrow ZZ$, as discussed above. However, since we are requiring the points to be away from the troublesome scenarios S_1 and S_2 , $\Gamma_{h_3 \rightarrow ZZ}^{m_3}$ generally takes small values. Accordingly, the total value $\Delta\Gamma_{h_3 \rightarrow ZZ}$ is essentially given by the contribution from $\Gamma_{h_3 \rightarrow ZZ}^{\text{mix}}$ (which explains the fact that the red points are almost entirely hidden under the green ones).

4.2.2 $h_3 \rightarrow h_1 Z$

The results for $h_3 \rightarrow h_1 Z$ are similar to those of $h_3 \rightarrow ZZ$, as can be seen in figure 5. For each combination, we apply the cuts associated to the blue points of the corresponding panel in figure 3. As

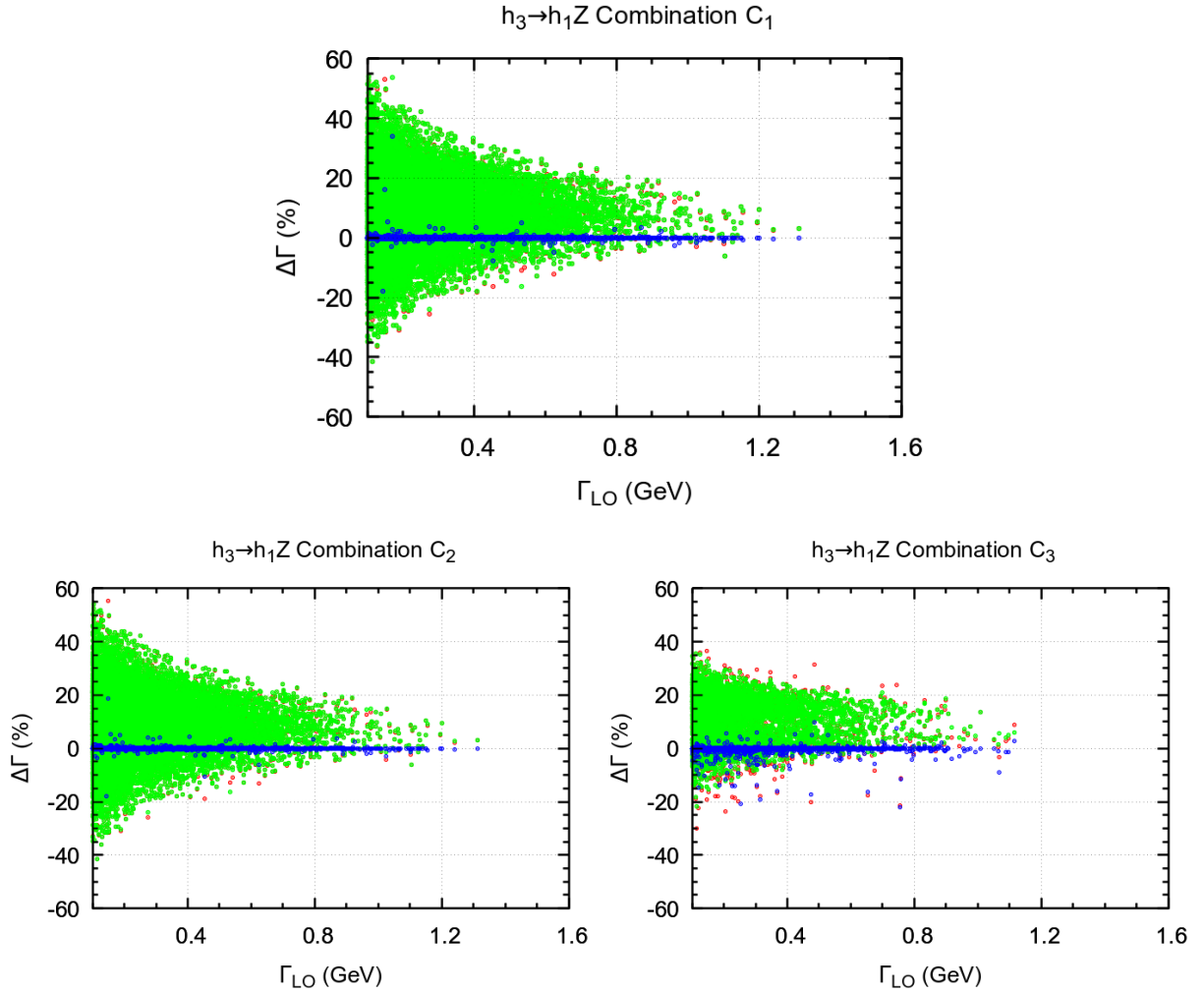


Figure 5: $\Delta\Gamma_{h_3 \rightarrow h_1 Z}$ in percentage against $\Gamma_{h_3 \rightarrow h_1 Z}^{\text{LO}}$, for the combinations C_1 (top), C_2 (bottom left) and C_3 (bottom right). The cuts leading to the blue points in figure 3 were applied. Only the interval $0.1 \text{ GeV} < \Gamma_{h_3 \rightarrow h_1 Z}^{\text{LO}} < 1.6 \text{ GeV}$ is shown. In red, $\Delta\Gamma_{h_3 \rightarrow h_1 Z}$; in green, $\Gamma_{h_3 \rightarrow h_1 Z}^{\text{mix}} / \Gamma_{h_3 \rightarrow h_1 Z}^{\text{LO}}$; in blue, $\Gamma_{h_3 \rightarrow h_1 Z}^{m_3} / \Gamma_{h_3 \rightarrow h_1 Z}^{\text{LO}}$. According to eq. 32, the red points are the sum of the green and the blue ones.

before, $\Gamma_{h_3 \rightarrow ZZ}^{m_3}$ generally takes small values.

4.2.3 $h_3 \rightarrow h_2 Z$

As already suggested, the decay $h_3 \rightarrow h_2 Z$ is significantly different from the other decays. This can be seen in figure 6, where we are using the same color code that was used in figures 4 and 5. For each combination, we apply the cuts associated to the green points of the corresponding panel in figure 3. Whereas in figures 4 and 5 the contribution from $\Gamma_j^{m_3}$ was small (so that the total relative correction

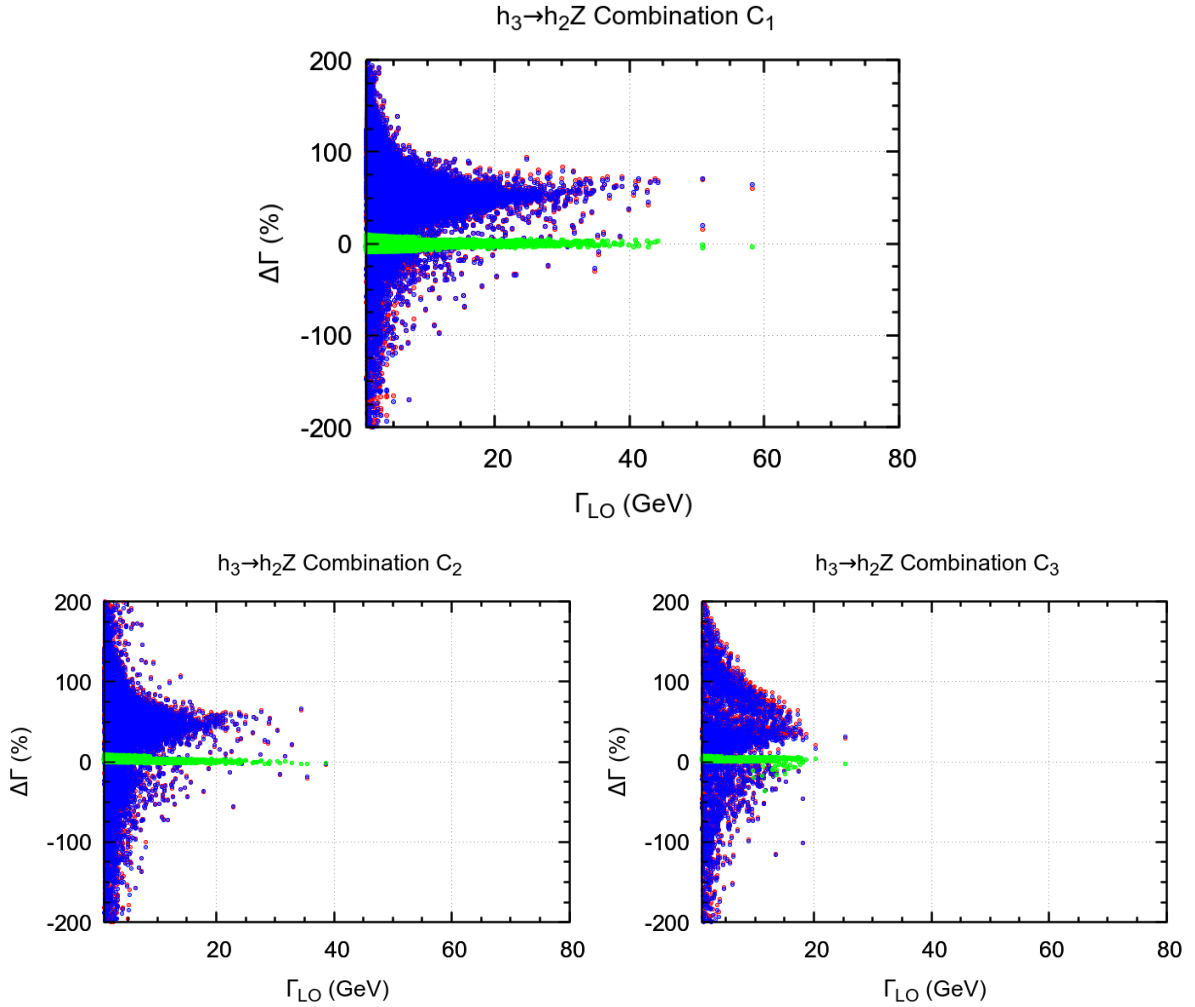


Figure 6: $\Delta\Gamma_{h_3 \rightarrow h_2 Z}$ in percentage against $\Gamma_{h_3 \rightarrow h_2 Z}^{\text{LO}}$, for the combinations C_1 (top), C_2 (bottom left) and C_3 (bottom right). The cuts leading to the green points in figure 3 were applied. Only the interval $1 \text{ GeV} < \Gamma_{h_3 \rightarrow h_2 Z}^{\text{LO}} < 80 \text{ GeV}$ is shown. In red, $\Delta\Gamma_{h_3 \rightarrow h_2 Z}$; in green, $\Gamma_{h_3 \rightarrow h_2 Z}^{\text{mix}}/\Gamma_{h_3 \rightarrow h_2 Z}^{\text{LO}}$; in blue, $\Gamma_{h_3 \rightarrow h_2 Z}^{m_3}/\Gamma_{h_3 \rightarrow h_2 Z}^{\text{LO}}$. According to eq. 32, the red points are the sum of the green and the blue ones.

$\Delta\Gamma_j$ was essentially given by the component Γ_j^{mix} , in figure 6 we have precisely the opposite: $\Gamma_{h_3 \rightarrow h_2 Z}^{\text{mix}}$ is relatively small, whilst $\Gamma_{h_3 \rightarrow h_2 Z}^{m_3}$ is by far the main contribution to $\Delta\Gamma_{h_3 \rightarrow h_2 Z}$. Moreover, whereas $\Delta\Gamma_j$ in the previous figures barely reached 40% (and only for very small values of Γ_j^{LO}), $\Delta\Gamma_{h_3 \rightarrow h_2 Z}$ can take values larger than that for the whole range of $\Gamma_{h_3 \rightarrow h_2 Z}^{\text{LO}}$.

Since it is evident that those very large values are a consequence of very large values of $\Gamma_{h_3 \rightarrow h_2 Z}^{m_3}$, we now

investigate this contribution. We can generically write $\Gamma_j^{m_3}$ as:

$$\Gamma_j^{m_3} = F_j \Delta m_3 \Gamma_j^{\text{LO}}. \quad (33)$$

Here, F_j is an LO (thus combination-independent) dimensionless factor, which depends only on the tree-level masses of the particles involved in the decay j . Eq. 33 implies that the contribution from $\Gamma_j^{m_3}$ to $\Delta\Gamma_j$ (blue points in figures 4, 5 and 6) is simply given by the product $F_j \Delta m_3$; that is,

$$\frac{\Gamma_j^{m_3}}{\Gamma_j^{\text{LO}}} = F_j \Delta m_3. \quad (34)$$

This means that the impact of $\Gamma_j^{m_3}$ on $\Delta\Gamma_j$ is given by the NLO correction Δm_3 weighted by the LO factor F_j . As a result, even if Δm_3 does not take large values (and so behaves perturbatively), the impact of $\Gamma_j^{m_3}$ on $\Delta\Gamma_j$ may end up being large (and so non-perturbative) if F_j turns out to be non-negligible. Now, from eq. 23c, one can read:

$$F_{h_3 \rightarrow h_2 Z} = -3 \frac{m_2^4 - m_{3R}^4 - 2m_2^2 m_Z^2 + m_Z^4}{m_{3R}^4 + m_2^4 + m_Z^4 - 2m_{3R}^2 m_2^2 - 2m_{3R}^2 m_Z^2 - 2m_2^2 m_Z^2}. \quad (35)$$

On the left plot of figure 7, we show $F_{h_3 \rightarrow h_2 Z}$ (in red) and Δm_3 (in green) against $\Gamma_{h_3 \rightarrow h_2 Z}^{\text{LO}}$ for the combination C_1 . We see that $F_{h_3 \rightarrow h_2 Z}$ always takes values larger than 5 for the whole range of $\Gamma_{h_3 \rightarrow h_2 Z}^{\text{LO}}$.

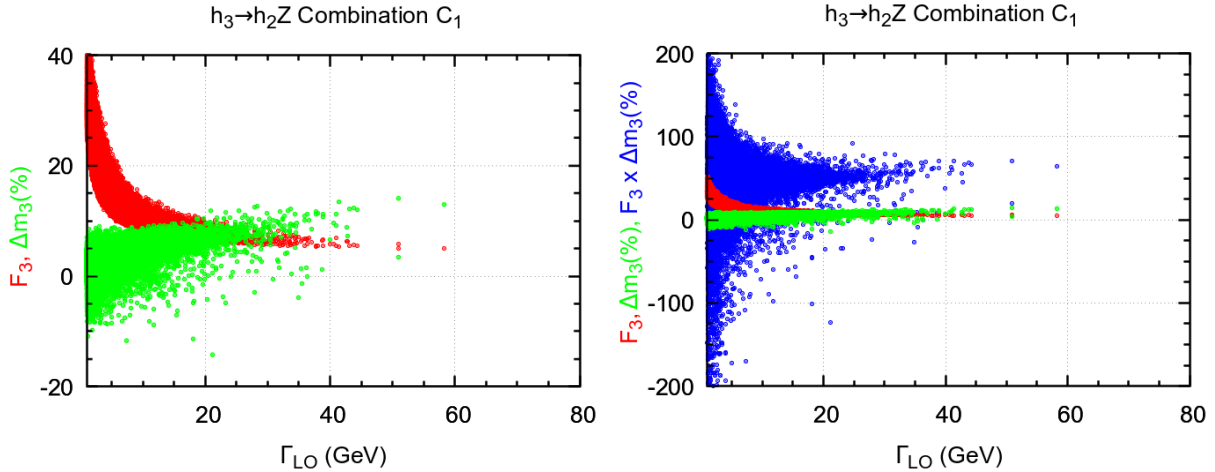


Figure 7: Left: $F_{h_3 \rightarrow h_2 Z}$ (red) and Δm_3 (green) against $\Gamma_{h_3 \rightarrow h_2 Z}^{\text{LO}}$ for the combination C_1 . Right: the same, but also with the product (blue) of the green and red points.

Hence, the impact of $\Gamma_{h_3 \rightarrow h_2 Z}^{m_3}$ on $\Delta\Gamma_{h_3 \rightarrow h_2 Z}$ is at least 5 times the NLO correction Δm_3 . This is clearly shown on the right plot, where the points in blue represent the product between the red and the green points (note that, according to eq. 34, those blue points are precisely the blue points on the top panel of figure 6). This explains the large values ($\gtrsim 40\%$) for $\Delta\Gamma_{h_3 \rightarrow h_2 Z}$ observed in figure 6. As we just suggested, these non-perturbative results do not stem from non-perturbative corrections to the h_3 mass; rather, even though such corrections take moderate values (green points in the left panel of figure 7), they end up being several times enhanced due to the peculiar LO factor $F_{h_3 \rightarrow h_2 Z}$.

4.2.4 $h_3 \rightarrow h_2 h_1$

The decay $h_3 \rightarrow h_2 h_1$ can be especially interesting, because its discovery would constitute an undoubtable sign of CP violation in the scalar sector (in the specific context of a 2HDM) [20, 59].¹⁹ In ref. [59], it was claimed that, at least for a very fine-tuned region of the parameter space, the process can have a branching ratio of about 3% at tree-level. We were not able to find such region. To be sure, we do find regions of theoretically valid points that lead to a tree-level branching ratio of the order of the percent level; only, they end up being ruled out by experimental results included in HIGGSBOUNDS5. This behaviour can be seen in figure 8, where we plot points with and without the constraints coming from HIGGSBOUNDS5. The figure clearly shows that, after applying such constraints, the branching ratio does not even reach 0.001%.

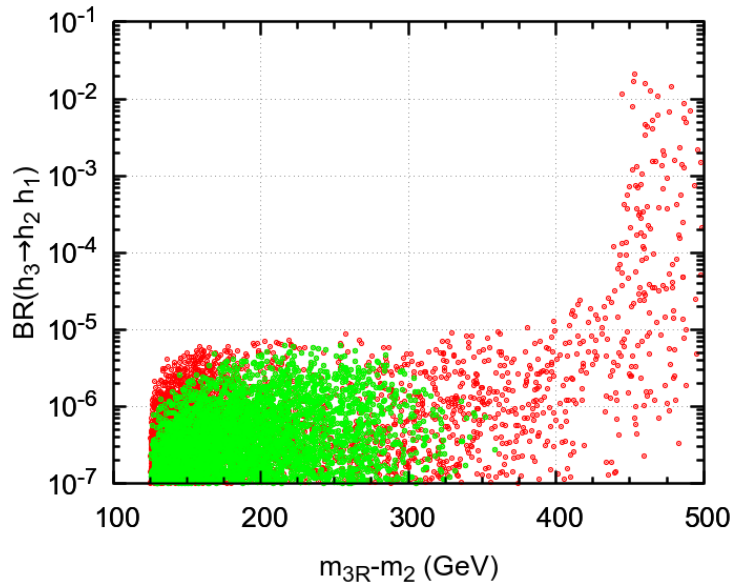


Figure 8: Tree-level branching ratio of $h_3 \rightarrow h_2 h_1$ against the difference $m_{3R} - m_2$. In red, points passing all constraints except HIGGSBOUNDS5; in green, points passing all constraints.

One might wonder whether the inclusion of one-loop effects may significantly change these results. Although it is expected that the contributions from eqs. 25 do not lead to big corrections to the tree-level decay width (as they are expected to show a perturbative behaviour), the one-loop corrections to m_{3R} could in principle lead to a broadening of the region of parameter space where the decay $h_3 \rightarrow h_2 h_1$ is kinematically allowed, which could allow regions with an enhanced decay width. We found that this is not the case; in fact, even considering the corrected h_3 mass, we can still find no regions of the parameter space leading to a relevant decay width for $h_3 \rightarrow h_2 h_1$.

5 Conclusions

We discussed NLO corrections to the derived mass m_3 of the heaviest neutral scalar h_3 in the C2HDM—one of the most simple models beyond the SM with CP violation in the scalar sector—and investigated the impact of such corrections in NLO decays of h_3 . Due to the presence of CP violation in the scalar

¹⁹This process does not necessarily imply CP violation in models other than the 2HDM [20].

sector of the C2HDM, the renormalization of the model requires the introduction of several non-physical parameters, so that one ends up having different possible combinations of independent counterterms for the same set of independent renormalized parameters. Restricting ourselves to four combinations, we found that the corrections to m_3 can be extremely large in all of them. The origin of problem lies in the particular dependence of m_3 on the independent parameters. Such dependence, in fact, leads to very large values in certain limits; this happens in such manner that, in very fine-tuned regions of the parameter space, the LO mass ends up assuming moderate values, whereas the NLO corrections become very large. We showed that, outside the fine-tuned regions, the corrections acquire moderate values.

We then investigated four specific NLO decay widths of h_3 . We stressed the existence of a contribution to those decay widths arising from the NLO corrections to the mass of h_3 . We showed that such contribution is small in $h_3 \rightarrow ZZ$ and $h_3 \rightarrow h_1 Z$, as long as the aforementioned fine-tuned regions are avoided. In the case of $h_3 \rightarrow h_2 Z$, however, there is a large superposition between those regions and the ones which kinematically allow the decay. As a consequence, the NLO corrections to the mass must become larger, although still perturbative; it turns out that a LO multiplicative factor enhances them, leading to NLO corrections to the decay width of the order of 50%. Finally, we discussed the process $h_3 \rightarrow h_2 h_1$; we showed that, although its discovery would constitute an irrefutable sign of CP violation in the scalar sector of a 2HDM, the current experimental results hinder relevant values for its decay width.

It would be of interest to explore the scenario where the renormalization of the model is performed by taking all the masses of the physical particles as independent parameters. One would then need to ascertain the behaviour of the counterterms; in particular, it would be relevant to investigate if there are regions of the parameter space for which the NLO corrections take large values, just as in the scenarios described in this paper.

Acknowledgments

We thank Sally Dawson, Ansgar Denner, Florian Domingo, Sebastian Paßehr, João P. Silva and Xiaoping Wang for discussions. DF is supported by the United States Department of Energy under Grant Contract DE-SC0012704; JCR is supported by Fundação para a Ciência e a Tecnologia (FCT, Portugal) through the projects CFTP-FCT Unit 777 (UIDB/00777/2020 and UIDP/00777/2020) and PTDC/FIS-PAR/29436/2017, which are partially funded through POCTI (FEDER), COMPETE, QREN and EU.

References

- [1] ATLAS Collaboration, G. Aad *et al.*, Phys.Lett. **B716**, 1 (2012), [1207.7214].
- [2] CMS Collaboration, S. Chatrchyan *et al.*, Phys.Lett. **B716**, 30 (2012), [1207.7235].
- [3] J. F. Gunion, H. E. Haber, G. L. Kane and S. Dawson, Front. Phys. **80**, 1 (2000).
- [4] I. P. Ivanov, Prog. Part. Nucl. Phys. **95**, 160 (2017), [1702.03776].
- [5] G. C. Branco *et al.*, Phys. Rept. **516**, 1 (2012), [1106.0034].
- [6] D. Fontes, M. Löschner, J. C. Romão and J. P. Silva, Eur. Phys. J. C **81**, 541 (2021), [2103.05002].
- [7] I. F. Ginzburg, M. Krawczyk and P. Osland, Two Higgs doublet models with CP violation, in *Linear colliders. Proceedings, International Workshop on physics and experiments with future electron-positron linear colliders, LCWS 2002, Seogwipo, Jeju Island, Korea, August 26-30, 2002*, pp. 703–706, 2002, [hep-ph/0211371], [,703(2002)].
- [8] W. Khater and P. Osland, Nucl. Phys. **B661**, 209 (2003), [hep-ph/0302004].
- [9] A. W. El Kaffas, W. Khater, O. M. Ogreid and P. Osland, Nucl. Phys. **B775**, 45 (2007), [hep-ph/0605142].
- [10] A. Wahab El Kaffas, P. Osland and O. M. Ogreid, Phys. Rev. **D76**, 095001 (2007), [0706.2997].
- [11] A. W. El Kaffas, P. Osland and O. M. Ogreid, Nonlin. Phenom. Complex Syst. **10**, 347 (2007), [hep-ph/0702097].
- [12] P. Osland, P. N. Pandita and L. Selbuz, Phys. Rev. **D78**, 015003 (2008), [0802.0060].
- [13] B. Grzadkowski and P. Osland, Phys. Rev. **D82**, 125026 (2010), [0910.4068].
- [14] A. Arhrib, E. Christova, H. Eberl and E. Ginina, JHEP **04**, 089 (2011), [1011.6560].
- [15] A. Barroso, P. M. Ferreira, R. Santos and J. P. Silva, Phys. Rev. **D86**, 015022 (2012), [1205.4247].
- [16] S. Inoue, M. J. Ramsey-Musolf and Y. Zhang, Phys. Rev. **D89**, 115023 (2014), [1403.4257].
- [17] K. Cheung, J. S. Lee, E. Senaha and P.-Y. Tseng, JHEP **06**, 149 (2014), [1403.4775].
- [18] D. Fontes, J. C. Romão and J. P. Silva, JHEP **12**, 043 (2014), [1408.2534].

- [19] C.-Y. Chen, S. Dawson and Y. Zhang, JHEP **06**, 056 (2015), [1503.01114].
- [20] D. Fontes, J. C. Romão, R. Santos and J. P. Silva, Phys. Rev. **D92**, 055014 (2015), [1506.06755].
- [21] D. Fontes *et al.*, JHEP **02**, 073 (2018), [1711.09419].
- [22] R. Boto, T. V. Fernandes, H. E. Haber, J. C. Romão and J. P. Silva, Phys. Rev. D **101**, 055023 (2020), [2001.01430].
- [23] K. Cheung, A. Jueid, Y.-N. Mao and S. Moretti, Phys. Rev. D **102**, 075029 (2020), [2003.04178].
- [24] D. Fontes and J. C. Romão, JHEP **06**, 016 (2021), [2103.06281].
- [25] D. Fontes, *Multi-Higgs Models: model building, phenomenology and renormalization*, PhD thesis, U. Lisbon (main), 2021, 2109.08394.
- [26] M. Frank, E. G. Fuakye and M. Toharia, 2112.14295.
- [27] A. D. Sakharov, Pisma Zh. Eksp. Teor. Fiz. **5**, 32 (1967), [Usp. Fiz. Nauk161,61(1991)].
- [28] CMS, S. Chatrchyan *et al.*, Phys. Rev. Lett. **110**, 081803 (2013), [1212.6639].
- [29] CMS, V. Khachatryan *et al.*, Phys. Rev. D **92**, 012004 (2015), [1411.3441].
- [30] ATLAS, G. Aad *et al.*, Phys. Lett. B **726**, 120 (2013), [1307.1432].
- [31] Particle Data Group, P. A. Zyla *et al.*, PTEP **2020**, 083C01 (2020).
- [32] E. Bagnaschi *et al.*, Eur. Phys. J. C **81**, 450 (2021), [2012.15629].
- [33] S. Heinemeyer and W. Hollik, Nucl. Phys. B **474**, 32 (1996), [hep-ph/9602318].
- [34] A. Brignole, J. R. Ellis, G. Ridolfi and F. Zwirner, Phys. Lett. B **271**, 123 (1991).
- [35] J. R. Ellis, G. Ridolfi and F. Zwirner, Phys. Lett. B **262**, 477 (1991).
- [36] A. Brignole and F. Zwirner, Phys. Lett. B **299**, 72 (1993), [hep-ph/9210266].
- [37] P. H. Chankowski, S. Pokorski and J. Rosiek, Nucl. Phys. B **423**, 497 (1994).
- [38] D. Fontes and J. C. Romão, Comput. Phys. Commun. **256**, 107311 (2020), [1909.05876].
- [39] N. D. Christensen and C. Duhr, Comput. Phys. Commun. **180**, 1614 (2009), [0806.4194].
- [40] A. Alloul, N. D. Christensen, C. Degrande, C. Duhr and B. Fuks, Comput. Phys. Commun. **185**, 2250 (2014), [1310.1921].
- [41] P. Nogueira, J. Comput. Phys. **105**, 279 (1993).
- [42] R. Mertig, M. Bohm and A. Denner, Comput. Phys. Commun. **64**, 345 (1991).
- [43] V. Shtabovenko, R. Mertig and F. Orellana, Comput. Phys. Commun. **207**, 432 (2016), [1601.01167].

- [44] V. Shtabovenko, R. Mertig and F. Orellana, Comput. Phys. Commun. **256**, 107478 (2020), [2001.04407].
- [45] T. Hahn and M. Perez-Victoria, Comput. Phys. Commun. **118**, 153 (1999), [hep-ph/9807565].
- [46] A. G. Akeroyd, A. Arhrib and E.-M. Naimi, Phys. Lett. **B490**, 119 (2000), [hep-ph/0006035].
- [47] I. F. Ginzburg and I. P. Ivanov, hep-ph/0312374.
- [48] S. Kanemura, T. Kubota and E. Takasugi, Phys. Lett. **B313**, 155 (1993), [hep-ph/9303263].
- [49] I. P. Ivanov and J. P. Silva, Phys. Rev. **D92**, 055017 (2015), [1507.05100].
- [50] O. Deschamps *et al.*, Phys. Rev. **D82**, 073012 (2010), [0907.5135].
- [51] F. Mahmoudi and O. Stal, Phys. Rev. **D81**, 035016 (2010), [0907.1791].
- [52] T. Hermann, M. Misiak and M. Steinhauser, JHEP **11**, 036 (2012), [1208.2788].
- [53] M. Misiak *et al.*, Phys. Rev. Lett. **114**, 221801 (2015), [1503.01789].
- [54] M. Misiak and M. Steinhauser, Eur. Phys. J. **C77**, 201 (2017), [1702.04571].
- [55] H. E. Haber and H. E. Logan, Phys. Rev. **D62**, 015011 (2000), [hep-ph/9909335].
- [56] ATLAS, G. Aad *et al.*, Phys. Rev. D **101**, 012002 (2020), [1909.02845].
- [57] P. Bechtle *et al.*, Eur. Phys. J. C **80**, 1211 (2020), [2006.06007].
- [58] ACME, V. Andreev *et al.*, Nature **562**, 355 (2018).
- [59] I. Low, N. R. Shah and X.-P. Wang, 2012.00773.